

Self-organized critical balanced networks: a unified framework

Mauricio Girardi-Schappo*,¹ Ludmila Brochini,² Ariadne A.

Costa,³ Tawan T. A. Carvalho,⁴ and Osame Kinouchi^{1,*}

¹*Universidade de São Paulo, FFCLRP,*

Departamento de Física, Ribeirão Preto, SP, Brazil

²*Universidade de São Paulo, Instituto de Matemática e Estatística, São Paulo, Brazil*

³*Universidade Federal de Goiás - Regional Jataí,*

Unidade Acadêmica Especial de Ciências Exatas, Jataí, GO, Brazil

⁴*Universidade Federal de Pernambuco,*

Departamento de Física, Recife, PE, Brazil

Abstract

Asynchronous irregular (AI) and critical states are two competing frameworks proposed to explain spontaneous neuronal activity. Here, we propose a mean-field model with simple stochastic neurons that generalizes the integrate-and-fire network of Brunel (2000). We show that the point with balanced inhibitory/excitatory synaptic weight ratio $g_c \approx 4$ corresponds to a second order absorbing phase transition usual in self-organized critical (SOC) models. At the synaptic balance point g_c , the network exhibits power-law neuronal avalanches with the usual exponents, whereas for nonzero external field the system displays the four usual synchronicity states of balanced networks. We add homeostatic inhibition and firing rate adaption and obtain a self-organized quasi-critical balanced state with avalanches and AI-like activity. Our model might explain why different inhibition levels are obtained in different experimental conditions and for different regions of the brain, since at least two dynamical mechanisms are necessary to obtain a truly balanced state, without which the network may hover in different regions of the presented theoretical phase diagram.

* osame@ffclrp.usp.br; girardi.s@gmail.com; These authors contributed equally to this work.

INTRODUCTION

Spontaneous brain activity happens in the form of nonlinear waves of action potentials that spread throughout the cortex. These waves are usually characterized by their sizes and duration under the critical brain hypothesis (see [1–3] for recent reviews), or by the underlying regularity and global synchronicity displayed by the firings of neuron populations under the balanced network hypothesis [4–6]. These two frameworks are often taken as discordant to each other [7], because a critical activity implies in long-range spatio-temporal correlations [8–10], whereas asynchronous irregular (AI) activity comes from Poissonian spike trains of interacting neurons [5, 6, 11].

Networks working at the critical point have the advantages of optimizing their dynamic range of response [12, 13], memory and learning processes [14, 15], computational power [16] and their flexibility to process information [17]. However, this highly susceptible state needs to be achieved and maintained spontaneously by an autonomous biological mechanism [18], introducing the problem of self-organized criticality (SOC). The attempts to model SOC in the context of neuronal networks involve mainly adaptive synapses [19, 20] and adaptive neuronal gains [21]. Both of these approaches are proven to have theoretically equivalent effects in the system’s phase space trajectory [21], resulting in a self-organized quasi-critical (SOqC) system. SOqC is a highly sensitive nearly-critical state able to maintain self-sustained activity, to reproduce the power-law exponents observed in experiments and produce large events (the “dragon kings”) [20–22]. Other authors claim that the power-laws in the brain are observed because experiments sample its activity long enough to average out its spatial disorder into a Griffiths phase [10, 23].

On the other hand, AI activity is intuitively expected to arise if the resting brain presented a statistically fair random noise. This state is characterized by irregular firing of individual neurons and global lack of synchronicity, leading Brunel [5] to conjecture AI, by visual inspection, as the typical spontaneous activity of the brain. This hypothesis is backed by theoretical evidence that AI states minimize redundancy [24] and speed-up the processing of inputs [5, 25], whereas excitation/inhibition (E/I) balanced networks may serve to construct high-dimensional population codes [26]. This situation is usually modeled by the so-called balanced networks, in which the system presents a transition from high to low, or even null, average activity [5] when the proportion, g , of excitatory to inhibitory synaptic strength is

varied. The transition point, $g_c = 4$, is called balanced because the excitatory population, corresponding to 80% of the neurons in the network (a fraction that is estimated from cortical data for glutamate-activated synapses [27]) is balanced by inhibitory synapses four times as strong as the excitatory ones.

Here, we introduce a model of an E/I network and show that the balanced point is a critical point usual for SOC models, unifying both approaches. Our model predicts that the balance point can be shifted away from the usual $g_c \approx 4$ for regimes in which synaptic couplings and neuronal gains are relatively small, keeping fixed the ratio of excitatory neurons in 80%. The balance point displays power-law avalanches with exponents that match experiments [28]. In fact, our model presents a critical line over the balance parameter when the average input over the network equals the average thresholds of the neurons. It also presents all the synchronicity states found by Brunel [5], namely the synchronous regular (SR), synchronous irregular (SI), asynchronous regular (AR), and AI. We determine the transition lines between these states. We also show that firing rate adaptation together with a homeostatic inhibition mechanism self-organizes the system towards a quasi-critical state – a fact that could explain the prevalence of E/I balanced states in many experiments [26]. Moreover, the introduced dynamic inhibition leading to the critical point may explain the enhancing of the dynamic range observed in experiments when inhibition is considered [29], since the critical state is known to optimize the dynamic range of excitable systems [12].

There have been attempts to model E/I networks in the context of criticality [30–33], and also connecting criticality to a synchronization phase transition [34]. However, all of these models have limitations that are naturally solved in our proposed framework. First, we present our model with all its features in detail, and we finish the paper comparing our framework to the existing ones.

THE MODEL

We use discrete-time stochastic integrate-and-fire neurons [35, 36]. A Boolean variable denotes if a neuron fires ($X[t] = 1$) or not ($X[t] = 0$) at time t . The membrane potentials

evolve (in discrete time) as:

$$\begin{aligned} V_i^E[t+1] &= \left[\mu V_i^E[t] + I_i^E[t] + \frac{1}{N} \sum_{j=1}^{N_E} W_{ij}^{EE} X_j^E[t] - \frac{1}{N} \sum_{j=1}^{N_I} W_{ij}^{EI} X_j^I[t] \right] (1 - X_i^E[t]), \\ V_i^I[t+1] &= \left[\mu V_i^I[t] + I_i^I[t] + \frac{1}{N} \sum_{j=1}^{N_E} W_{ij}^{IE} X_j^E[t] - \frac{1}{N} \sum_{j=1}^{N_I} W_{ij}^{II} X_j^I[t] \right] (1 - X_i^I[t]), \end{aligned} \quad (1)$$

where $N = N_E + N_I$ is the total number of neurons, μ is a leakage parameter and $I_i[t]$ are external inputs. Here the indices E and I denote the excitatory and inhibitory populations. A link W_{ij}^{EI} means a synapse from an inhibitory neuron to an excitatory neuron (the second index is always the presynaptic one), and the same rule applies to W^{EE} , W^{II} and W^{IE} . Notice that if some neuron fires at time t , in the next time step its voltage is reset to zero due to the factor $(1 - X_i[t])$. Also, the inhibitory character of the synapses is given by the negative sign in front of the summations: the W^{EI} and W^{II} are always absolute positive values. We notice that our network is a complete graph, instead of the sparse network examined by Brunel [5]. However, we will show that there is no qualitative difference between the two phase diagrams of both models.

The individual neurons fire following a piecewise linear probability function (see Fig. 1a):

$$P(X = 1 | V) \equiv \Phi(V) = \Gamma(V - \theta) \Theta(V - \theta) \Theta(V_S - V) + \Theta(V - V_S), \quad (2)$$

where Γ is the neuronal gain, θ is a firing threshold, $V_S = \theta + 1/\Gamma$ is the saturation potential and $\Theta(x)$ is the step Heaviside function. The fact that $0 < \Phi(V) < 1$ in the interval $[\theta, V_S]$ means that the spikes are stochastic, a feature that intends to model the effects of membrane noises. Notice that the limit $\Gamma \rightarrow \infty$ reproduces the (discrete time) deterministic integrate-and-fire neuron with hard threshold $V_S = \theta$.

RESULTS

First, we show that the balance point is a critical point, characterizing its critical exponents and its avalanche distributions. We then determine the full phase diagram, locating the synchronicity states (SR, AR, AI, SI). And finally, we introduce an adaptive dynamics in the inhibitory synapses together with firing rate adaptation and show that the system then hovers towards the critical balanced point.

The mean-field limit

In the Methods section, we derive an expression for the mean firing rate of the excitatory and inhibitory neuronal populations to be used here. We approximate the excitatory/inhibitory synaptic weights by their average values, $W^{EI} = \langle W_{ij}^{EI} \rangle$ (for all the E/I combinations), and write the firing densities (the fraction of active sites) $\rho_E = 1/N_E \sum_j X_j^E$ and $\rho_I = 1/N_I \sum_j X_j^I$. We write the fractions of excitatory and inhibitory neurons as $p = N_E/N$ and $q = 1 - p = N_I/N$, respectively. We also consider only the case with a stationary average input $I = \langle I_i[t] \rangle$, so that the neurons' membrane voltages evolve as:

$$\begin{aligned} V_i^E[t+1] &= [\mu V_i^E[t] + I + pW^{EE}\rho_E[t] - qW^{EI}\rho_I[t]] (1 - X_i^E[t]) , \\ V_i^I[t+1] &= [\mu V_i^I[t] + I + pW^{IE}\rho_E[t] - qW^{II}\rho_I[t]] (1 - X_i^I[t]) . \end{aligned} \quad (3)$$

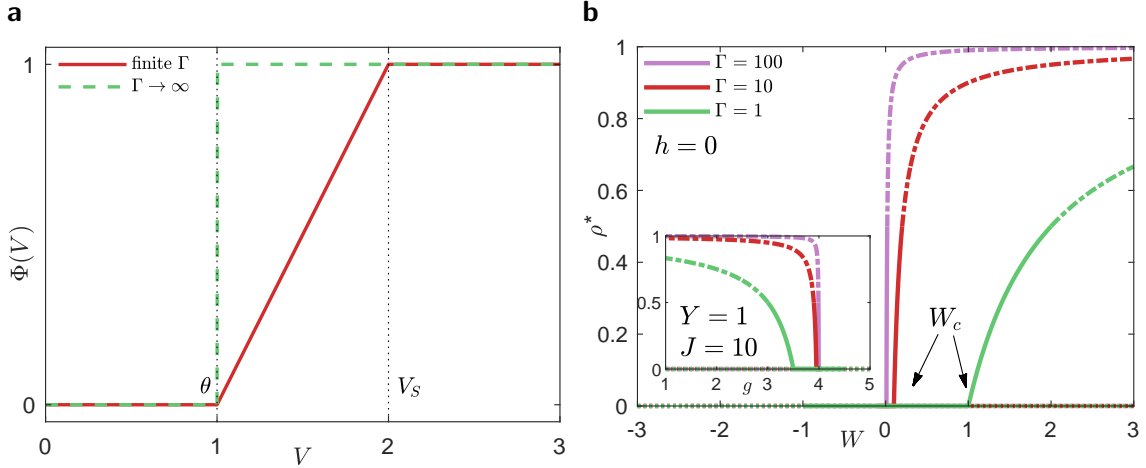


FIG. 1. Firing probability function $\Phi(V)$ and continuous phase transition. **a**, Solid: soft firing threshold $\theta = 1$ with neuronal gain $\Gamma = 1$, so that the saturation voltage is $V_S = \theta + 1/\Gamma = 2$. Dashed: in the $\Gamma \rightarrow \infty$ limit, we recover the deterministic leaky integrate-and-fire (LIF) model with a sharp threshold $\theta = V_S = 1$. **b**, Phase transition for $\rho^* = \rho_E = \rho_I$ as a function of W along the line $h = 0$, for $\Gamma = 1, 10$ and 100 and $J = 10$ ($W_c = 1/\Gamma$). **b (inset)**, Phase transition for ρ^* as a function of the ratio g along the line $Y = 1$ for the same Γ and J . The order parameter ρ^* is equivalent to the firing frequency ν_0 of Brunel model [5]. Notice that the FP with $\rho^* > 1/2$ (dot-dashed) represents cycle-2 due to the refractory period of one time step (Brunel's Synchronous Regular SR state).

The densities ρ_E and ρ_I of firing neurons are our order parameters (similar to the firing frequency ν_0 of the Brunel model [5]) and the synaptic weights W^{EE}, W^{EI}, W^{IE} and W^{II} are our control parameters. Together with p, I, μ, θ and Γ , we have a nine-dimensional parameter space that will be further reduced.

Analytical results are exact for $\mu = 0$. The case $0 < \mu < 1$ admits numerical results for any leakage μ [22, 36], but also has analytical solutions close to the phase transition. For $\rho \geq 1/2$, solutions are independent of μ . Here, we consider the case $\mu = 0$ since it captures all the important dynamics of the model and the effect of non-zero μ is described in the Methods. Making the E/I synaptic strengths uniform (Brunel’s model A [5]), we can study the stationary states in terms of the synaptic balance parameter g : we define $W^{EE} = W^{IE} = J$, $W^{II} = W^{EI} = gJ$, and the weighted synaptic weight, $W = pJ - qgJ$. This choice gives us a uniform solution (see Methods) $\rho[t] = \rho_E[t] = \rho_I[t]$ that evolves as:

$$\rho[t + 1] = \Gamma (1 - \rho[t]) (W\rho[t] + I - \theta) \Theta(W\rho[t] + I - \theta). \quad (4)$$

Its fixed points are given by:

$$\Gamma W \rho^2 + (1 + \Gamma h - \Gamma W) \rho - \Gamma h = 0, \quad (5)$$

where we defined the supra-threshold external current, $h = I - \theta$, equivalent to an external field in usual SOC models.

In order to put Brunel’s model [5] into the standard SOC framework given in the parameter space (W, h) (Fig. 2a), we introduce the parameter $Y = I/\theta$ – the fractional external current – entirely equivalent to Brunel’s input ratio $\nu_{\text{ext}}/\nu_{\text{thr}}$ where ν_{ext} is the average of a noisy input current and ν_{thr} is proportional to θ . We assume $\theta = 1$ without loss of generality. Also, recall that $g = p/q - W/(qJ)$, enabling the study of the system in the *balanced notation* phase diagram (g, Y) (Fig. 2b). At this point we have a six dimensional parameter space $\{\Gamma, J, g, Y, \mu, p\}$, but we fix $p = 0.8$, and hence $q = 0.2$, from cortical data [27]. We henceforth call this the static model. If any of the parameters presented in this section is allowed to vary with time, then we have the dynamic model that will be discussed later in this manuscript.

Balanced point as a second order critical point

Considering the case $h = I - \theta = 0 \equiv h_c$ in equation (5), we obtain an absorbing state $\rho^0 = 0$ (the quiescent phase, Q) which is stable for $W < W_c \equiv 1/\Gamma$, and an active solution (also called H or L for high or low activity, respectively):

$$\rho^* = \frac{\Gamma W - 1}{\Gamma W} = \frac{W - W_c}{W}, \quad (6)$$

stable for $W > W_c$. This is a transcritical bifurcation usual in SOC models, see Fig. 1b. Equation (6) is exact for $\mu = 0$. For $\mu > 0$, $h_c = -\mu$, and a good approximation near the phase transition results in $W_c = (1 - \mu)/\Gamma$, such that

$$\rho^* = \frac{W - W_c}{W}(1 - \mu). \quad (7)$$

For $W \rightarrow W_c$, the active solution reduces to $\rho^* \sim (W - W_c)^\beta$, with $\beta = 1$ being the critical exponent associated with the coupling intensity. Analogously, we can isolate h from equation (5) and expand for small ρ (due to small external h) on the critical point $W = W_c$ to obtain $\rho^* \sim [h/W_c]^{1/\delta_h}$ with $\delta_h = 2$ the critical exponent associated with the external field. The susceptibility, χ , exponent is obtained by taking the derivative of ρ with respect to h at $h = 0$ in equation (5), using $\Gamma = 1/W_c$, and expanding for $W \rightarrow W_c$. This procedure results in $\chi \sim |W - W_c|^{-\gamma'}$ with $\gamma' = 1$. These mean field exponents are compatible with the directed percolation (DP) universality class [37], the framework proposed to govern SOC systems [21, 22, 36, 38]. In the DP, the variance of the network activity defines the exponent γ by $\text{Var}(\rho) \sim |W - W_c|^{-\gamma}$ with $\gamma = 0$ [37]. This explains the jump in the coefficient of variation of the network activity observed by Brunel [5], since a zero-valued γ exponent indicates a discontinuous jump in the variance of ρ .

In the balanced notation, for the external input $Y_c = h_c + 1 = 1$, and using the relationship between W and g , we can write the critical point as:

$$g_c = p/q - \frac{1}{q\Gamma J} = 4 - \frac{1}{0.2\Gamma J}, \quad (8)$$

where we chose the usual fractions $p = 0.8$ and $q = 0.2$ for cortical neurons. Our result generalizes the known condition $g_c \approx 4$: If the term $1/(q\Gamma J)$ turns out significant, the transition shifts towards lower values of g (see the inset of Fig. 1b). This means that when the synaptic strengths, J , or the firing rate gains, Γ , are small, the network will not need

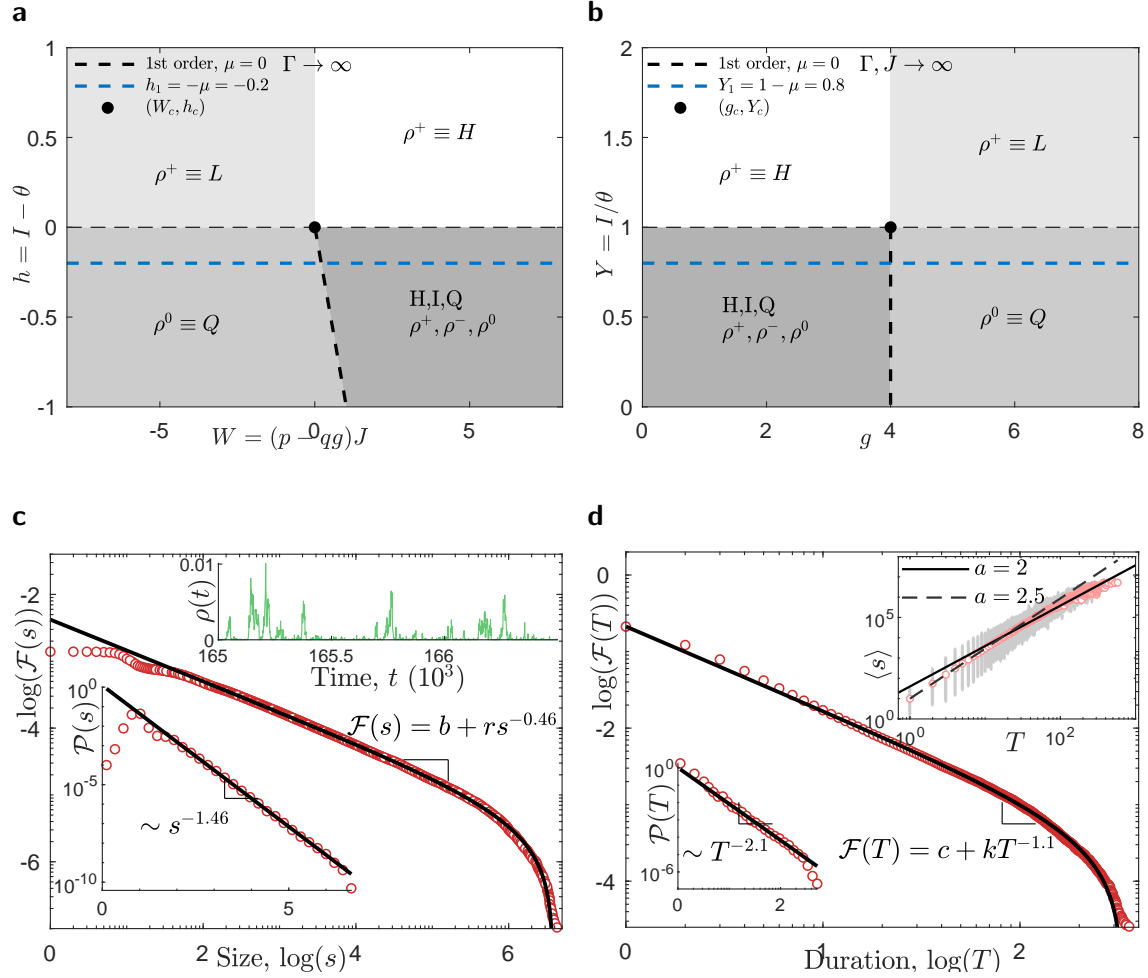


FIG. 2. Phase diagrams for large ΓJ and critical avalanches in the balanced point of the static model. **a**, Phase diagram in the (W, h) plane. Notice that the Low (L) and High (H) behavior corresponds to a single phase ρ^+ with different amplitudes. **b**, Phase diagram in the balanced notation, (g, Y) plane. The critical point lies at $(W_c = 0, h_c = 0)$ or $(g_c = 4, Y_c = 1)$ [bullet, equation (8)]. The Q phase loses stability at the horizontal dashed line $Y_c = 1 - \mu$ (or $h_c = -\mu$); we show $\mu = 0$ (black and thin dashed line) and $\mu = 0.2$ (blue dashed line). This diagram should be compared to Brunel's Fig. 1A [5]. **c**, Time series of network activity density (top inset), distribution (bottom inset) and complementary CDF (main plot) of avalanche sizes in the static model, yielding $\tau = 1.46$ (solid line). **d**, Avalanche size and duration scaling law yields two exponents, $a = 2.5$ for small avalanches and $a = 2$ for the rest of the data (top inset), distribution (bottom inset) and complementary CDF (main plot) of avalanche duration in the static model, yielding $\tau_t = 2.1$ (solid line). Note the deviation of the distributions for small and short avalanches, causing the cross-over effect in the $\langle s \rangle \sim T^a$ scaling law.

much inhibition, hence the smaller g value. This was only observed numerically in [5]. The large ΓJ regime, which approximates the LIF neurons in equation (2), recovers the usual balanced condition, $g_c \approx 4$, obtained by Brunel [5].

Rewriting equation (6) using g_c , we get:

$$\rho^* = \frac{pJ - qgJ - 1/\Gamma}{pJ - qgJ} = \frac{g_c - g}{p/q - g}, \quad (9)$$

and we recover the phase transition for $g \rightarrow g_c$ with $\beta = 1$ and $\gamma' = 1$. Nevertheless, the states are flipped in the g -axis: the active state now happens for $g < g_c$. The expansion for $Y \gtrsim Y_c \equiv 1$ at $g = g_c$ also yields $\delta_h = 2$. The same holds for $\mu > 0$, but with $Y_c = 1 - \mu$. So, balanced networks share the same second order phase transition of SOC models.

Avalanches in the balanced critical point

The balanced point (which is now proven to be a DP critical point) displays avalanche-like activity that can be measured from the $\rho[t]$ time series (see the top inset of Fig. 2c). We simulate the static model as a mean-field network of $N = 10^6$ neurons with $\Gamma = 1$, $J = 10$, $g = g_c = 3.5$, $Y = Y_c = 1$, $\mu = 0$ and $p = 0.8$. We define an avalanche as the sum of all the spikes between two consecutive silent absorbing states [39]. Avalanches are sparked independently when the activity goes to zero. We fit cutoff power laws to the complementary cumulative distributions (CDF) of avalanche sizes, $\mathcal{F}(s) \equiv \mathcal{P}(S > s) = b + rs^{-\tau+1}$, and duration, $\mathcal{F}(T) \equiv \mathcal{P}(T' > T) = c + kT^{-\tau_t+1}$ (b , r , c and k are fit constants related to the cutoff of the power laws [40]). This representation provides a clearer visualization of the data, because it is a continuous function of its variables; it also has very reduced noise, its precision does not depend on the size of the bins of the distribution's histogram, and it has a better defined cutoff [40].

Least squares fit yields $\tau = 1.46(4)$ and $\tau_t = 2.1(1)$ for avalanche sizes and duration exponents, respectively (main plots of Figs. 2c and 2d). We also fit the histogram of sizes, $\mathcal{P}(s) \sim s^{-\tau}$, and duration, $\mathcal{P}(T) \sim T^{-\tau_t}$, and obtain the same values for τ and τ_t (bottom insets of Figs. 2c and 2d). The expected values for these exponents in the DP universality class are $\tau_{\text{DP}} = 1.5$ and $\tau_{t,\text{DP}} = 2$, but the finite-size effects cause the deviation of the distributions for small s and short T , biasing the fitted values of the exponents. Nevertheless, both the fitted values and the theory values match experiments [28].

The average avalanche size scales with avalanche duration according to $\langle s \rangle \sim T^a$ such that $a = (\tau_t - 1)/(\tau - 1)$ [37, 39, 41]. The theoretical value of a in DP is $a_{DP} = 2$. In our simulation, we observe a cross-over in the $\langle s \rangle$ vs. T data (top inset of Fig. 2d), such that for large and long avalanches $a = 2$ (exactly equal to the theory), and for small and short avalanches, $a = 2.5$ due to the finite-size deviations in the $\mathcal{P}(s)$ and $\mathcal{P}(T)$ distributions. The fitted values $\tau = 1.46$ and $\tau_t = 2.1$ result in $a_{\text{fit}} = 2.4$, which is between the cross-over exponents, hence agreeing with the $\langle s \rangle$ vs. T data.

The synaptic balance vs. external current phase diagram

The solutions to equation (5) for $h \neq 0$ (or $Y \neq 1$) are:

$$\rho^\pm = \frac{\Gamma W - \Gamma h - 1 \pm \sqrt{(\Gamma W - \Gamma h - 1)^2 + 4\Gamma^2 W h}}{2\Gamma W}, \quad (10)$$

The balanced notation can be recovered letting $h = Y - 1$ (recall that $\theta = 1$) and $W = pJ(1 - g\gamma)$, where $\gamma = q/p$ (not to be confused with the critical exponent for the variance of ρ):

$$\rho^\pm = \frac{1 - g\gamma - (Y - 1)/(pJ) - 1/(p\Gamma J) \pm \sqrt{\Delta}}{2(1 - g\gamma)}, \quad (11)$$

$$\Delta \equiv \left[1 - g\gamma - \frac{Y - 1}{pJ} - \frac{1}{p\Gamma J} \right]^2 + 4(1 - g\gamma) \frac{Y - 1}{pJ}.$$

Notice that there is no divergence when $g = p/q$ ($W = 0$) because equation (5) then gives $\rho = \Gamma h/(1 + \Gamma h)$. Solutions for equation (11) are plotted in Figs. 3a and 3b for different values of g and Y . Equation (11) yields the activity states of high and low activity (H and L, the ρ^+), and also the intermediary state (I, the unstable ρ^- branch). However, there is also a stable quiescent solution Q, $\rho^0 = 0$, for $Y \leq Y_c$ due to the step function in equation (4); but Q is unstable over the critical line for $Y_c = 1 - \mu$ if $g < g_c$ due to the transcritical bifurcation at the critical point (horizontal dashed lines in Fig. 2b).

For $Y < Y_c$, there is a first order transition line where the ρ^+ branch appears and start to coexist with the stable ρ^0 solution, generating the intermediary unstable state ρ^- through a fold bifurcation (Fig. 3a). The first order transition line, shown in Fig. 3c, is (see Methods):

$$Y_1(g) = 1 - \frac{1}{\Gamma} \left[\sqrt{p\Gamma J(1 - g\gamma)} - 1 \right]^2. \quad (12)$$

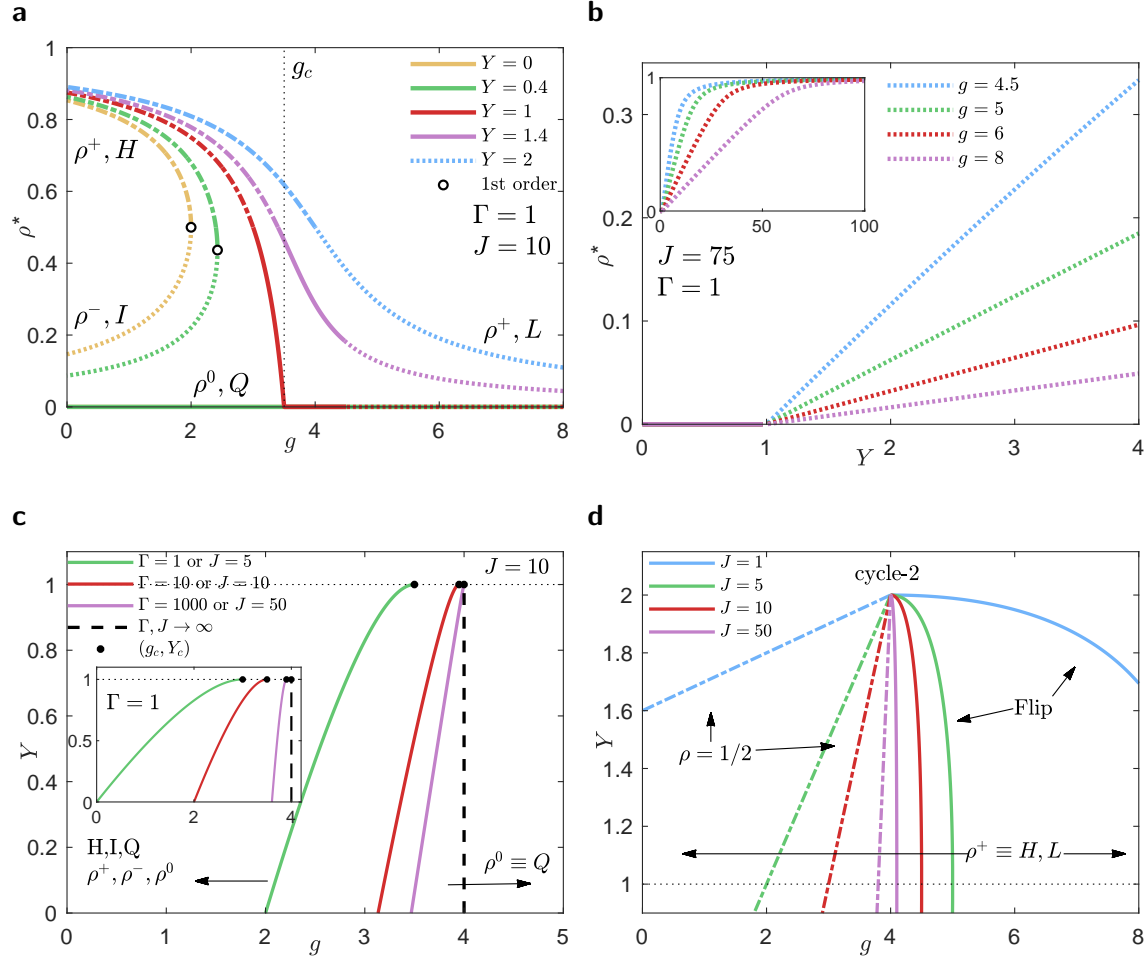


FIG. 3. **Firing density ρ vs. g and Y and phase diagrams in the plane (g, Y) .** **a**, Firing density as a function of g for many Y [equation (11)], highlighting the activity states H for high, L for low (both corresponding to ρ^+), I for the intermediary and unstable ρ^- (originating in a fold bifurcation, or first order phase transition) and Q for $\rho = 0$. **b**, Firing density as a function of Y for many g ; linear behavior occurs for small Y , but saturates for large external current (inset). This plot has no SR behaviour and should be compared to Fig. 1B (right) in Ref. [5]. The dotted lines for ρ^+ in both panels **a** and **b** correspond to marginally stable fixed points. **c**, First order phase transition (fold bifurcation) lines [equation (12)] for $J = 10$ and many neuronal gains Γ ; below the line $Y = 1$, we have the Q state, whereas to the left of each Y_1 line we also have the states H and I. **c (inset)**, Same diagram as in the main plot, but for $\Gamma = 1$ and many synaptic intensities J . **d**, Bifurcation lines for $\Gamma = 1$ towards cycle-2 at $\rho^+ = 1/2$, equation (13) (dot-dash line), and flip [equation (14), solid line]. SR occurs above each $\rho^+ = 1/2$ line and SI occurs above each flip line.

This transition depends on J and Γ and it ends at $Y_1(g_c) = Y_c = 1$. For large ΓJ , we recover Brunel's [5] diagram, with an almost vertical Y_1 line at g_c , as shown in Fig. 2b.

For $Y > Y_c$, the ρ^- (I) solution disappears and the Q phase is unstable. The ρ^+ solution varies continuously from H to L activity state. There is no phase transition by changing g , although a clear change of behavior (large derivative) occurs close to g_c . This happens because, for $g < g_c$, we have a supercritical phase with self-sustained activity being fueled by the external input (the H state) whereas for the $g > g_c$ region, there is no self-sustained activity (Fig. 3a), making the L state appear due entirely to the external current. Nevertheless, both the H and L states bifurcate (see Fig. 3d) giving rise to distinct oscillatory behaviors to be discussed in the next section.

Even though equation (11) admits H solutions that have $\rho^+ > 1/2$ as a stable fixed point, the original system does not. This happens because the neurons defined in equation (3) have a refractory period of 1 time step (since $\Phi(0) \equiv 0$), yielding a maximum firing rate of $\rho = 1/2$. Thus, mean-field solutions that have $\rho^+ > 1/2$ correspond to a cycle-2 dynamics of the form $\rho[t+1] = 1/2 - \rho[t]$ for the network. The amplitude of this cycle depends on the initial condition, so $\rho > 1/2$ is marginally stable. The transition line towards this cycle-2 dynamics is given by (see Methods):

$$Y_{SR}(g) = \frac{pJ}{2}(1 - g\gamma) + 1 + \frac{1}{\Gamma}. \quad (13)$$

This curve is plotted in Fig. 3d for different values of J . When ΓJ is large, it becomes almost vertical, turning almost all the H state into cycle-2 activity for $g < g_c$. This transition is not a standard bifurcation of maps, but rather a particularity of the model raised by the refractory period.

The L state bifurcates through a flip. The consequence is that the $\rho[t]$ map given in equation (4) starts to cycle between negative and positive values, even though the negative ones are turned to $\rho = 0$ due to the step function. The bifurcation line is given by (see Methods):

$$Y_F(g) = 1 - \frac{1}{\Gamma} + pJ(g\gamma - 1) + \frac{2}{\Gamma} \sqrt{1 - p\Gamma J(g\gamma - 1)}. \quad (14)$$

This curve is shown in Fig. 3d for different values of J . It becomes almost vertical for large ΓJ , turning almost all the L state into oscillations for $g > g_c$.

Spiking patterns emerging for external input currents

The H and L activity states (both given by ρ^+) can be further split into four different states, depending on the global synchronicity and local regularity of the firing patterns of the network. The network may or may not be globally synchronized; and the synchronization (or the lack of it) may happen in a locally regular or irregular fashion (meaning that each individual neuron either spikes regularly or not, respectively) [5]. Thus, we have the four different oscillatory states: globally synchronous and locally regular (SR); globally asynchronous and locally regular (AR); asynchronous and irregular (AI); and synchronous irregular (SI).

Fig. 4a shows the location of each of these four states in the complete phase diagram of our model for finite ΓJ . The main feature defining the synchronicity of the SR and SI states is that the frequency of the firing density oscillations is well-defined, meaning that the network is indeed operating as a global oscillator. The firing density of AR and AI states, on the other hand, behaves mostly as noise.

The mean-field solutions to equation (11) give us only the global state of synchrony. To probe for the microscopic regularity in spiking patterns, we simulated equation (3) for a network of $N = 10^6$ neurons, $J = 10$, $\Gamma = 1$, $p = 0.8$, $\mu = 0$, $Y = 1.2$ and four values of g : $g = 3.0$ (excitation-dominated network), $g = 3.5$ (weakly excitation-dominated network), $g = 4.3$ (weakly inhibition-dominated network), and $g = 4.7$ (inhibition dominated network). To obtain slow oscillations, we simulated a large leakage regime, $\mu = 0.9$, with a small input current, $I = 0.001$, giving $Y = 0.101$ (recalling that the critical line is at $Y_c = 1 - \mu = 0.1$), in the inhibition-dominated region of the diagram, $g = 4.5$. The (g, Y) points for $\mu = 0$ are marked in Fig. 4a, and the results of the simulations are shown Fig. 4b.

The self-sustained activity regime, when summed up to the external current, gives rise to regular microscopic behavior, SR and AR. The AR state turns into SR as excitation is increased when the system undergoes the $\rho = 1/2$ transition (see Fig. 4a). Note that this is not a standard bifurcation for map systems, but rather a particular feature of our model due to its 1 ms refractory period, causing the marginally stable cycle-2 activity.

The addition of an external current to the quiescent regime generates irregular microscopic activity. This happens because interactions are dominated by inhibitory synapses, such that the negative currents transmitted through the network compensate for the average

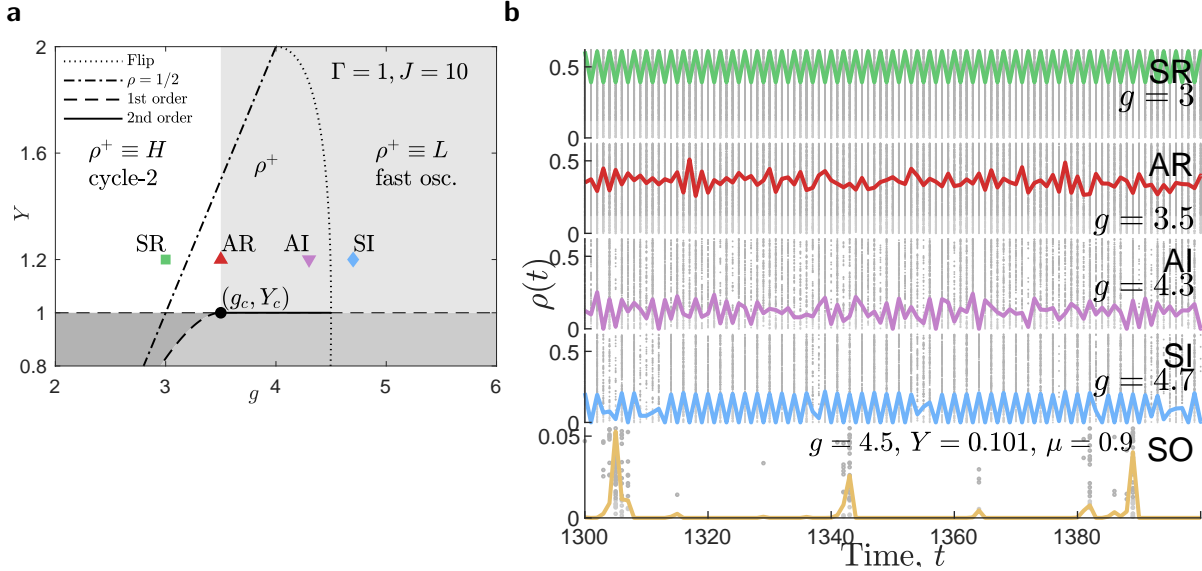


FIG. 4. **Spiking patterns.** **a**, Full phase diagram of our model for $\mu = 0$, $\Gamma = 1$, $J = 10$, $Y = 1.2$, and finite ΓJ ; from left to right we have the synchronous regular (SR/cycle-2, $g = 3$), asynchronous regular (AR/ ρ^+ /High, $g = 3.5$), asynchronous irregular (AI/ ρ^+ /Low, $g = 4.3$) and synchronous irregular (SI/fast oscillations, $g = 4.7$). **b**, Network simulation results, showing the firing density time series, $\rho[t]$, and the raster plot of 1000 neurons for the cases highlighted in panel **a**. **b (bottom)**, Example of slow oscillations (SO). They appear as sparse avalanches close to $Y = 1 - \mu$. Parameters are the same as in panel **a**, except for $\mu = 0.9$ and $Y = 0.101$.

external positive input. The AI state turns into SI as inhibition is increased when the system undergoes a flip bifurcation (see Fig. 4a). From then on, the system is so saturated with inhibition that the activity often dies out just to be sparked again by the constant input, generating fast oscillations that, globally, look almost like cycle-2.

Differently from Brunel [5], all our model's randomness is condensed in the stochastic firing of individual neurons. The network is topologically regular (a full graph), and the synaptic and external inputs are homogeneous parameters. Thus, the only requirements to generate these four behaviors are: an intrinsic noise source, and a refractory period that is equal to or larger than the synaptic transmission time (which is 1 ms in our model).

When leakage is introduced into the model through $\mu > 0$, the voltage of the neurons become distributed in an exponential way due to the slow recovery of the membrane potential

after the spike [36]. This generates a chain of delayed firings intercalated by long periods of silence that depend on μ . The firings form sparse relatively large avalanches intertwined with small avalanches, and Brunel [5] called them as slow oscillations (SO, bottom panel of Fig. 4). This behavior occurs for external input Y very close to the critical line $Y \gtrsim Y_c = 1 - \mu$. Large inputs saturate the activity either through regular or irregular states, depending on the value of g .

Self-organized critical balanced networks

For the brain to reach and maintain the balanced state with $g = g_c$ and $Y = Y_c$ without fine tuning, there has to exist a self-organizing mechanism. While inhibition frequently increases together with excitation after the stimulation of a neuron, the reverse does not seem to happen; that is, excitation does not compensate for inhibition when the neuron is suppressed [26]. To model this feature, we introduce an adaptive mechanism on the weights of the inhibitory synapses inspired on the Levina-Herrmann-Geisel (LHG) dynamics [19],

$$W_{ij}^{II}[t+1] = W_{ij}^{II}[t] + \frac{1}{\tau_W}(A - W_{ij}^{II}[t]) + u_W W_{ij}^{II}[t]X_j[t], \quad (15)$$

$$W_{ij}^{EI}[t+1] = W_{ij}^{EI}[t] + \frac{1}{\tau_W}(A - W_{ij}^{EI}[t]) + u_W W_{ij}^{EI}[t]X_j[t]. \quad (16)$$

Here, τ_W is a (large) recovery time, A is a recovery level and u_W is the fraction of the synaptic strength facilitated when a presynaptic neuron fires. This mechanism potentiates inhibition by a factor u_W when the presynaptic neuron fires and then relaxes with a time scale given by τ_W . The dynamics in the W_{ij} generates a response in the g axis of the phase diagram through $g_{ij}^{EI/II}[t] = W_{ij}^{EI/II}[t]/J$.

However, our model has two degrees of freedom, requiring another independent mechanism to reach the balanced condition autonomously. This is achieved through firing rate adaptation [42], which we model by a homeostatic dynamics in the firing threshold of the neurons:

$$\theta_i[t+1] = \theta_i[t] - \frac{1}{\tau_\theta}\theta_i[t] + u_\theta\theta_i[t]X_i[t], \quad (17)$$

where the parameter u_θ is the fractional increase in the neuron threshold after it fires, and τ_θ is a recovery time scale towards a null theta relative to the external current. This dynamics is sufficient to drive the system along the Y axis, because $Y_i[t] = I/\theta_i[t]$. When the neuron

fires, its threshold adapts to prevent new firings, otherwise it decays with a large time scale τ_θ .

In the long-term, the proposed dynamics generates adaptation relative to the input level of the network around the mean activity, given by $\bar{g}^{II} = \overline{\langle g_{ij}^{II}[t] \rangle}$, $\bar{g}^{EI} = \overline{\langle g_{ij}^{EI}[t] \rangle}$, and $\bar{Y} = \overline{\langle Y_i[t] \rangle}$, where the top bar denotes a long-time average and the brackets $\langle \cdot \rangle$ denote an average over the individual activity of the neurons. We simulated a network of $N = 10^3$ neurons over a long time ($10^4\text{ms}=10\text{s}$) with static parameters $\Gamma = 1$, $J = 10$, $\mu = 0$, $p = 0.8$, and dynamic parameters $\tau_W = \tau_\theta = 100$, $A = 73.5$, $u_W = u_\theta = 0.1$. In this regime, the balance point of the static model is $g_c = 3.5$ and $Y_c = 1$. In contrast, the activity of the dynamic model had averages $\bar{g}^{II} = \bar{g}^{EI} = 3.53(2)$ and $\bar{Y} = 1.01(2)$, where the digit in parentheses corresponds to the error associated to the last digit (see Fig. 5a).

The system self-organized very close to the critical balanced point of the static model (Fig. 5b). However, note that $\bar{g}^{II/EI}$ and \bar{Y} are slightly deviated towards the AI region (*i.e.* $\bar{g}^{II/EI} \gtrsim g_c$ and $\bar{Y} \gtrsim Y_c$, compare Fig. 5b with the phase diagram in Fig. 4a). This is confirmed the visual inspection of the network activity (Fig. 5c), showing a global desynchronized state with local irregular firing pattern.

DISCUSSION

We presented a model of an E/I network that has a balanced condition between excitation and inhibition when $g = g_c$. The balanced point, g_c , may be shifted away from the previously theoretical value $g_c \approx 4$ due to the soft threshold of the stochastic neurons, keeping the same fraction of excitatory to inhibitory neurons in the network ($p = 0.8$ for excitatory neurons, similar to the average fraction of glutamate-activated synapses in the brain [27]).

Other authors studied E/I network models and also found continuous phase transitions happening at points resembling criticality [30–33], and also connecting criticality to a synchronization phase transition [34]. However, all of these models have limitations that are naturally solved in our proposed framework. The model by Poil *et al.* [30] does not seem to present true criticality, since its exponents vary widely according to the models' parameters [33], and they do not follow the proper scaling law for critical systems [33, 37, 39, 41]. Even though Lombardi *et al.* [31] also modeled homeostatic mechanisms, their avalanche sizes do not correspond closely to experiments neither to DP, and the avalanche distribu-

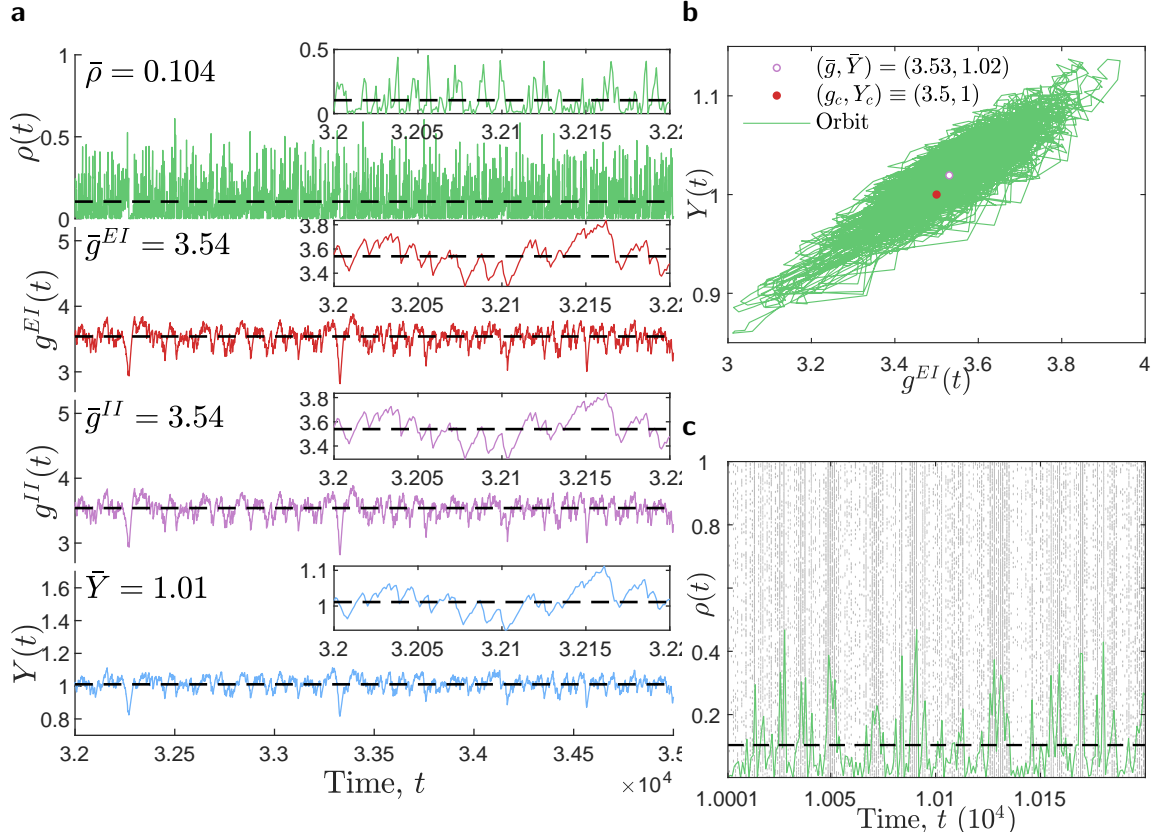


FIG. 5. **Self-organization towards the balanced critical point.** Parameters: $\tau_W = \tau_\theta = 100$, $A = 73.5$, $u_W = u_\theta = 0.1$, $\Gamma = 1$ and $J = 10$. **a**, Time series for $\rho[t]$, $g^{EI}[t] = \langle W_{ij}^{EI}[t] \rangle / J$, $g^{II}[t] = \langle W_{ij}^{II}[t] \rangle / J$ and $Y[t] = I / \langle \theta_i[t] \rangle$. The $\rho[t]$ large peaks are dragon king events. **a (inset)**, Details with a smaller time scale. **b**, Self-organization trajectories in the g vs. Y plane. The system hovers around the critical balanced point of the static model, $g_c = 3.5$ and $Y_c = 1$, where neuronal avalanches occur. The time-series average (red dot) is $\bar{g}^{II/EI} = 3.53(2)$, $\bar{Y} = 1.02(2)$. **c**, Raster plot for 1000 neurons of the data in panel **a**. Visually, the activity resembles the AI state, but avalanches occur and vertical bands correspond to dragon kings (very large) avalanches.

tions follow power laws only for very small inhibition [32]. Di Santo *et al.* [34] studied a phenomenological model of a spiking network and found AI and critical states, but they do not consider E/I populations independently, neither they derive the rate equations from a microscopic model [34].

In contrast, our model: a) generalizes the balance point from the standard Brunel model [5], showing that it pertains to the expected DP universality class of SOC systems [37];

b) displays the power-law scaling for avalanche sizes and duration on the balanced critical point matching experiments [28]; c) contains all the four synchronicity states predicted by Brunel [5] when external input is considered; d) self-organizes towards the critical point via the adaptation of inhibitory synapses [26] and firing rates [42], both of which are known to occur in the brain; e) the self-organized point displays quasi-critical avalanches and a microscopic dynamics that resembles, through visual inspection, AI activity. Thus, we unify in a single framework all observed the features from critical neuronal network states with all the features of balanced networks, giving rise to a self-organized (quasi-)critical balanced network.

The levels of the adaption mechanisms are controlled by their respective time scales and fraction of potentiation. The two required dynamics give the system a good deal of freedom in the display of macroscopic activity. For instance, low levels of firing rate adaptation could drive the system towards either a switching between different synchronicity-regularity states for $Y > 1$ (say, switching between SR and AR, or AR and AI, or even AI and SI), or a self-organized bistable [43] dynamics due to the discontinuous transition for $Y < 1$. On the other hand, low levels of inhibition adaptation could generate long periods of high activity intertwined with periods of low activity. Therefore, our model could explain how drugs that modulate these mechanisms can change the global activity of the considered system; and it could also explain why different regions of the brain display different activity patterns, as discussed in [5] and [26] and in references therein, due to different levels of adaptability. Nevertheless, if both mechanisms are strong, the system will be driven towards the balanced critical point, although the effective distance of the dynamics to the true static critical point is controlled by the time scales of the dynamics via gross tuning [20–22, 36]: the larger the time scales, the less fluctuations around the underlying critical point are observed.

Our network is topologically regular (full graph), the synaptic delays are fixed (1ms) and homogeneous, and the refractory period of 1ms comes from the definition of the neurons' dynamics. In fact, all the parameters of our model are homogeneous. Thus, the SR, AR, AI and SI states are purely derived from the intrinsic stochasticity of the firing of the neurons modeled by the $\Phi(V)$ function. This function is an abstraction of all the possible noise sources happening on the neuron's membrane. Although it is implied that the stochastic processes on the membrane of the neurons have to occur in a time scale smaller than the refractory period and synaptic delays of the system.

Even though we study a full graph and Brunel studies a sparse random network [5], both models share the same type of results because the author assumes that there is no correlations in the system other than those induced by a global firing rate [5]. Then, his results are also in the mean-field limit due to the high dimensionality of the network, and the critical exponents we found also apply to his model in the balanced point. In fact, the universality of critical phenomena guarantees that our results apply to any network with high dimensionality that keeps the same collective behavior, the symmetries, and the conservation laws of our model [44].

The simulation of large systems with the self-organizing mechanism is limited mainly by memory due to the number of variables that need to be kept for every time step of the dynamics (of the order of TN^2 , where T is the total number of time steps in the simulation). However, our results serve as proof of concept, since increasing N is known to enhance the convergence to the critical (and balanced) point [20, 22]. Other limitation is the purely stochastic description of the spikes. Nevertheless, if the time scales and dynamical features of the neurons and synapses are obeyed, our results are robust due to universality [44].

We have unified the balanced networks framework and the neuronal avalanches SOC framework into a single formalism. Even though the model needs deeper exploration, the general scenario is clear: standard balanced networks are a special case of the absorbing state SOC models in DP universality class (those with large ΓJ), and SOC models in DP are a particular case of standard balanced networks (those with field $Y = 1$). And homeostatic mechanisms in the system's inhibition and firing rate adaptation drives the network towards a quasi-critical that displays power-law avalanches and AI-like firing pattern.

-
- [1] Janina Hesse and Thilo Gross. Self-organized criticality as a fundamental property of neural systems. *Front. Syst. Neurosci.*, 8:166, 2014.
 - [2] Luca Cocchi, Leonardo L Gollo, Andrew Zalesky, and Michael Breakspear. Criticality in the brain: A synthesis of neurobiology, models and cognition. *Prog. Neurobio.*, 158:132–152, 2017.
 - [3] J Wilting and V Priesemann. 25 years of criticality in neuroscience – established results, open controversies, novel concepts. *arXiv preprint arXiv:1903.05129*, 2019.
 - [4] Rob R. de Ruyter van Steveninck, Geoffrey D. Lewen, Steven P. Strong, Roland Koberle, and

- William Bialek. Reproducibility and variability in neural spike trains. *Science*, 275:1805–1808, 1997.
- [5] Nicolas Brunel. Dynamics of sparsely connected networks of excitatory and inhibitory spiking neurons. *J. Comput. Neurosci.*, 8(3):183–208, 2000.
- [6] Alexander S. Ecker, Philipp Berens, Georgios A. Keliris, Matthias Bethge, Nikos K. Logothetis, and Andreas S. Tolias. Decorrelated neuronal firing in cortical microcircuits. *Science*, 327:584–587, 2010.
- [7] Jens Wilting and Viola Priesemann. Inferring collective dynamical states from widely unobserved systems. *Nat. Commun.*, 9(1):2325, 2018.
- [8] K Linkenkaer-Hansen, V V Nikouline, J M Palva, and R J Ilmoniemi. Long-range temporal correlations and scaling behavior in human brain oscillations. *J. Neurosci.*, 21(4):1370–1377, 2001.
- [9] A Haimovici, E Tagliazucchi, P Balenzuela, and D R Chialvo. Brain organization into resting state networks emerges at criticality on a model of the human connectome. *Phys. Rev. Lett.*, 110:178101, 2013.
- [10] Mauricio Girardi-Schappo, Germano S Bortolotto, Jheniffer J Gonsalves, Leonel T Pinto, and Marcelo H R Tragtenberg. Griffiths phase and long-range correlations in a biologically motivated visual cortex model. *Sci. Rep.*, 6:29561, 2016.
- [11] W. R. Softky and C Koch. The highly irregular firing of cortical cells is inconsistent with temporal integration of random epsps. *J. Neurosci.*, 13:334–350, 1993.
- [12] Osame Kinouchi and Mauro Copelli. Optimal dynamical range of excitable networks at criticality. *Nat. Phys.*, 2(5):348–351, 2006.
- [13] Woodrow L Shew, Hongdian Yang, Thomas Petermann, Rajarshi Roy, and Dietmar Plenz. Neuronal avalanches imply maximum dynamic range in cortical networks at criticality. *J. Neurosci.*, 29(49):15595–15600, 2009.
- [14] Lucilla de Arcangelis, Carla Perrone-Capano, and Hans J Herrmann. Self-organized criticality model for brain plasticity. *Phys. Rev. Lett.*, 96(2):028107, 2006.
- [15] Bruno Del Papa, Viola Priesemann, and Jochen Triesch. Criticality meets learning: Criticality signatures in a self-organizing recurrent neural network. *PLoS One*, 12:e0178683, 2017.
- [16] J M Beggs and N Timme. Being critical of criticality in the brain. *Front. Physiol.*, 3:163, 2012.

- [17] Thiago S Mosqueiro and Leonardo P Maia. Optimal channel efficiency in a sensory network. *Phys. Rev. E*, 88(1):012712, 2013.
- [18] Juan A Bonachela, Sebastiano de Franciscis, Joaquín J Torres, and Miguel A Muñoz. Self-organization without conservation: are neuronal avalanches generically critical? *J. Stat. Mech.*, 2010(02):P02015, 2010.
- [19] Anna Levina, J Michael Herrmann, and Theo Geisel. Dynamical synapses causing self-organized criticality in neural networks. *Nat. Phys.*, 3(12):857–860, 2007.
- [20] Ariadne A Costa, Mauro Copelli, and Osame Kinouchi. Can dynamical synapses produce true self-organized criticality? *J. Stat. Mech.*, 2015(6):P06004, 2015.
- [21] Osame Kinouchi, Ludmila Brochini, Ariadne A Costa, Campos. Joo G F, and Mauro Copelli. Stochastic oscillations and dragon king avalanches in self-organized quasi-critical systems. *Sci. Rep.*, 9:3874, 2019.
- [22] Ariadne A Costa, Ludmila Brochini, and Osame Kinouchi. Self-organized supercriticality and oscillations in networks of stochastic spiking neurons. *Entropy*, 19(8):399, 2017.
- [23] Paolo Moretti and Miguel A Muñoz. Griffiths phases and the stretching of criticality in brain networks. *Nat. Commun.*, 4:2521, 2013.
- [24] A. Hyvärinen and E. Oja. Independent component analysis: algorithms and applications. *Neural Netw.*, 13:411–430, 2000.
- [25] Carl van Vreeswijk and Haim Sompolinsky. Chaos in neuronal networks with balanced excitatory and inhibitory activity. *Science*, 274(5293):1724–1726, 1996.
- [26] Sophie Denève and Christian K Machens. Efficient codes and balanced networks. *Nat. Neurosci.*, 19:375–382, 2016.
- [27] Peter Somogyi, Gábor Tamás, Rafael Lujan, and Eberhard H. Buhl. Salient features of synaptic organisation in the cerebral cortex. *Brain Res. Rev.*, 26:113–135, 1998.
- [28] John M Beggs and Dietmar Plenz. Neuronal avalanches in neocortical circuits. *J. Neurosci.*, 23(35):11167–11177, 2003.
- [29] Bao hua Liu, Ya tang Li, Wen pei Ma, Chen jie Pan, Li I. Zhang, and Huizhong Whit Tao. Broad inhibition sharpens orientation selectivity by expanding input dynamic range in mouse simple cells. *Neuron*, 71:542–554, 2011.
- [30] Simon-Shlomo Poil, Richard Hardstone, Huibert D Mansvelder, and Klaus Linkenkaer-Hansen. Critical-state dynamics of avalanches and oscillations jointly emerge from balanced excita-

- tion/inhibition in neuronal networks. *J. Neurosci.*, 32(29):9817–9823, 2012.
- [31] F. Lombardi, H. J. Herrmann, C. Perrone-Capano, D. Plenz, and L. de Arcangelis. Balance between excitation and inhibition controls the temporal organization of neuronal avalanches. *Phys. Rev. Lett.*, 108:228703, 2012.
- [32] F. Lombardi, H. J. Herrmann, and L. de Arcangelis. Balance of excitation and inhibition determines 1/f power spectrum in neuronal networks. *Chaos*, 27:047402, 2017.
- [33] Leonardo Dalla Porta and Mauro Copelli. Modeling neuronal avalanches and longrange temporal correlations at the emergence of collective oscillations: Continuously varying exponents mimic M/EEG results. *PLoS Comput. Biol.*, 15:e1006924, 2019.
- [34] Serena di Santo, Pablo Villegas, Raffaella Burioni, and Miguel A Muñoz. Landau–Ginzburg theory of cortex dynamics: Scale-free avalanches emerge at the edge of synchronization. *Proc. Natl. Acad. Sci. USA*, 115(7):E1356–E1365, 2018.
- [35] Antonio Galves and Eva Löcherbach. Infinite systems of interacting chains with memory of variable length a stochastic model for biological neural nets. *J. Stat. Phys.*, 151(5):896–921, 2013.
- [36] Ludmila Brochini, Ariadne A Costa, Miguel Abadi, Antônio C Roque, Jorge Stolfi, and Osame Kinouchi. Phase transitions and self-organized criticality in networks of stochastic spiking neurons. *Sci. Rep.*, 6:35831, 2016.
- [37] Miguel A. Muñoz, Ronald Dickman, Alessandro Vespignani, and Stefano Zapperi. Avalanche and spreading exponents in systems with absorbing states. *Phys. Rev. E*, 59(5):6175, 1999.
- [38] Ronald Dickman, Alessandro Vespignani, and Stefano Zapperi. Self-organized criticality as an absorbing-state phase transition. *Phys. Rev. E*, 57(5):5095, 1998.
- [39] Mauricio Girardi-Schappo and Marcelo H. R. Tragtenberg. Measuring neuronal avalanches in disordered systems with absorbing states. *Phys. Rev. E*, 97:042415, 2018.
- [40] Mauricio Girardi-Schappo, Osame Kinouchi, and Marcelo H R Tragtenberg. Critical avalanches and subsampling in map-based neural networks coupled with noisy synapses. *Phys. Rev. E*, 88(2):024701, 2013.
- [41] Germano S. Bortolotto, Mauricio Girardi-Schappo, Jheniffer J. Gonsalves, Leonel T. Pinto, and Marcelo H. R. Tragtenberg. Information processing occurs via critical avalanches in a model of the primary visual cortex. *J. Phys. Conf. Ser.*, 686(1):012008, 2016.
- [42] Jan Benda and Andreas V. M. Herz. A universal model for spike-frequency adaptation. *Neural*

Comput., 15:2523–2564, 2003.

- [43] Serena di Santo, Raffaella Burioni, Alessandro Vezzani, and Miguel A Muñoz. Self-organized bistability associated with first-order phase transitions. *Phys. Rev. Lett.*, 116(24):240601, 2016.
- [44] Géza Ódor. Universality classes in nonequilibrium lattice systems. *Rev. Mod. Phys.*, 76(3):663–724, 2004.

ACKNOWLEDGEMENTS

This article was produced as part of the activities of FAPESP Research, Innovation and Dissemination Center for Neuromathematics (Grant No. 2013/07699-0, S. Paulo Research Foundation). We acknowledge financial support from CNPq, FACEPE, and Center for Natural and Artificial Information Processing Systems (CNAIPS)-USP. L.B. thanks FAPESP (Grant No. 2016/24676-1). A.A.C. thanks FAPESP (Grants No. 2016/00430-3 and No. 2016/20945-8). M.G.-S. thanks FAPESP (Grant No. 2018/09150-9).

AUTHOR CONTRIBUTIONS

M.G.-S., A.A.C. and T.T.A.C. performed the simulations. O.K., L.B. and M.G.-S. made the analytic calculations. M.G.-S. and O.K. wrote the manuscript.

COMPETING INTERESTS

The authors declare no competing financial and non-financial interests.

METHODS

A. Mean-field approximation

The mean-field approximation is exact for our complete graph network. From the definition of the firing function, $\Phi(V)$, the model may have two types of stationary states: the active state, such that $\rho_E = \rho_I \equiv \rho^* > 0$, and the quiescent Q state, $\rho_E = \rho_I \equiv \rho^0 = 0$. At

instant $t + 1$, the active population is simply given by the integral over V of $\Phi(V)P_t^{E/I}(V)$ – recalling that $\Phi(V)$ is the conditional probability of firing given V :

$$\rho_{E/I}[t + 1] = \int_{\theta}^{\infty} \Phi(V) P_t^{E/I}(V) dV \quad (18)$$

This relation is sufficient for deriving the fixed point equation for ρ when $\mu = 0$.

The evolution of firing rates can also be described in terms of the neuronal *firing ages* in the case $\mu > 0$ [21, 36]. This is possible because the reset of the potential causes a population of neurons that fire together to also evolve together until they fire again. We call $U_k^E[t]$ the potential of a certain population of excitatory neurons that fired k time steps before time t and $\eta_k^E[t]$ the proportion of such neurons with respect to the excitatory population. Then, the proportion of firing excitatory neurons evolves as:

$$\rho^E[t + 1] = \sum_{k=0}^{\infty} \Phi(U_k^E[t]) \eta_k^E[t]. \quad (19)$$

A neuron with firing age k at time t can, at time $t + 1$, either fire with probability $\Phi(U_k^E[t])$ or become part of the population with firing age $k + 1$ of proportion $\eta_{k+1}^E[t + 1]$. In the latter case, potentials and proportions evolve as:

$$\eta_{k+1}^E[t + 1] = (1 - \Phi(U_k^E[t])) \eta_k^E[t] \quad (20)$$

$$U_{k+1}^E[t + 1] = \mu U_k^E[t] + I[t] + pW^{EE} \rho_E[t] - qW^{EI} \rho_I[t], \quad (21)$$

Where $U_0^E[t] = 0$ for any t (since the reset potential is zero). By writing equivalent relations for the inhibitory population, we obtain recurrence equations that describe the evolution of the whole system after a reasonably short transient that guarantees that every neuron has fired (or has had zero potential) at least once, allowing us to perform numerical studies of the system in the mean field framework.

B. The absorbing quiescent state

Let us determine the stability boundary of the Q (ρ^0) phase. In the stationary state of equation (22), the distribution of voltages has a single Dirac peak. When $V < \theta$, we have the inactive state reducing equation (3) to:

$$V_i^{E/I}[t + 1] = \mu V_i^{E/I}[t] + I, \quad (22)$$

which has the stationary solution $V[t + 1] = V[t] \equiv V_1$ given by

$$V_1 = \frac{I}{1 - \mu}, \quad (23)$$

$$P_\infty(V) = \delta(V - V_1). \quad (24)$$

Since the equations (22) and (23) hold for both E or I neurons, we dropped the E/I superscripts. Neurons start to fire when $V_1 > \theta$, so the stability boundary line for the Q phase, given by $V_1 = \theta$, corresponds to the dashed line $Y_0 = I_0/\theta = 1 - \mu$ in Fig. 2.

C. The zero leakage case

For $\mu = 0$, the distribution of potentials $P_\infty(V)$ presents only two Dirac peaks. The system in $V = 0$ (the reset) has a population $\rho_{E/I}[t]$ and the other, in $V = V_1^{E/I}$, has a population $(1 - \rho_{E/I}[t])$:

$$P_t^{E/I}(V) = \rho_{E/I}[t]\delta(V) + (1 - \rho_{E/I}[t])\delta(V - V_1^{E/I}[t]), \quad (25)$$

where the $V_1^{E/I}[t]$ are now given by:

$$\begin{aligned} V_1^E[t] &= I + pW^{EE}\rho_E[t] - qW^{EI}\rho_I[t], \\ V_1^I[t] &= I + pW^{IE}\rho_E[t] - qW^{II}\rho_I[t]. \end{aligned} \quad (26)$$

The firing densities $\rho_E[t]$ and $\rho_I[t]$ evolve as:

$$\begin{aligned} \rho_E[t + 1] &= \int \Phi(V) P_t^E(V) dV \\ &= (1 - \rho_E[t]) [\Gamma(V_1^E - \theta) \Theta(V_1^E - \theta) \Theta(V_S - V_1^E) + \Theta(V_1^E - V_S)], \\ \rho_I[t + 1] &= \int \Phi(V) P_t^I(V) dV \\ &= (1 - \rho_I[t]) [\Gamma(V_1^I - \theta) \Theta(V_1^I - \theta) \Theta(V_S - V_1^I) + \Theta(V_1^I - V_S)]. \end{aligned} \quad (27)$$

For large input current I , we may have $V_1^{E/I} > V_S$ and we have:

$$\rho_{E/I}[t + 1] = (1 - \rho_{E/I}[t]) \Theta(V_1^{E/I}[t] - V_S) = (1 - \rho_{E/I}[t]). \quad (28)$$

This admits marginally stable cycle-2 solutions (*i.e.* they have no basins of attraction) [36]. Equation (28) has an average $\langle \rho[t] \rangle = 1/2$. This fixed point corresponds to a synchronized regular (SR) state [5].

When $V_1^{E/I} < V_S$, we have:

$$\rho_{E/I}[t+1] = \Gamma \left(V_1^{E/I}[t] - \theta \right) (1 - \rho_{E/I}[t]) \Theta(V_1^{E/I}[t] - \theta), \quad (29)$$

For Brunel's [5] Model A ($W^{EE} = W^{IE} = J$, $W^{II} = W^{EI} = gJ$), and using the weighted synaptic strength $W = pJ - qgJ$, we get:

$$\rho_{E/I}[t+1] = \Gamma (W\rho_{E/I}[t] + h) (1 - \rho_{E/I}[t]) \Theta(W\rho_{E/I}[t] + h), \quad (30)$$

where we defined the field (suprathreshold current) $h = I - \theta$.

1. The bistable phase

The bistable phase is composed of a stable branch H (ρ^+), an unstable branch I (ρ^-) and the quiescent branch Q (ρ^0). In the phase diagram, the bistable phase is separated from a phase where the quiescent state is unique through a fold bifurcation. To determine this phase boundary, we return to the solution for the ρ^\pm fixed points:

$$\rho^\pm = \frac{1 - g\gamma - (Y - 1)/(pJ) - 1/(p\Gamma J) \pm \sqrt{\Delta}}{2(1 - g\gamma)}, \quad (31)$$

$$\Delta \equiv (1 - g\gamma - (Y - 1)/(pJ) - 1/(p\Gamma J))^2 + 4(1 - g\gamma)(Y - 1)/(pJ).$$

We locate the transition line $g_1(Y)$ where the two branches appear by using the condition $\Delta = 0$. We get:

$$g_1 = \frac{p}{q} - \frac{1}{qJ\Gamma} \left[1 + \sqrt{\Gamma(1 - Y)} \right]^2. \quad (32)$$

This enters the phase diagram (g, Y) in Fig. 3 as a first order transition line. That means that there is no H or L states for $g > g_1$ and $Y < 1 - \mu$, only the quiescent Q state, which is fully compatible with Brunel's phase diagram [5].

The first order transition line can also be written as:

$$Y_1(g, \Gamma, J) = 1 - \frac{1}{\Gamma} \left[\sqrt{p\Gamma J(1 - g\gamma)} - 1 \right]^2, \quad (33)$$

such that we recover the diagram of Brunel [5], with an almost vertical line Y_1 crossing $Y = 1$ at $g_1 = g_c$ for large ΓJ (see Fig. 3c).

The corresponding first order transition lines in the SOC notation are:

$$\Gamma_1(W, h) = \left[\frac{1}{\sqrt{W}} - \frac{1}{\sqrt{-2h}} \right]^2, \quad (34)$$

$$h_1(\Gamma, W) = -\frac{1}{\Gamma} \left[\sqrt{\Gamma W} - 1 \right]^2, \quad (35)$$

$$W_1(\Gamma, h) = \frac{1}{\Gamma} \left[1 + \sqrt{-\Gamma h} \right]^2. \quad (36)$$

The last relation is fully compatible with equation (32), which can be read as $W_1 = qJ(p/q - g_1)$. At the bifurcation point, the first order transition step is given by:

$$\Delta\rho = \rho^+ - \rho^0 = \frac{\sqrt{-\Gamma h}}{1 + \sqrt{-\Gamma h}} = \frac{\sqrt{\Gamma(1-Y)}}{1 + \sqrt{\Gamma(1-Y)}}, \quad (37)$$

which is consistent with the continuous phase transition in the limit $h \rightarrow 0$ (see Fig. 3a).

2. Transition between regular spiking states

The asynchronous regular (ρ^+ or AR) phase turns into a cycle-2 (synchronous regular, SR) if its activity achieves the value $\rho = 1/2$ as the excitation is increased. This occurs because the neurons have a refractory period of one time step, and the maximum firing rate of a single neuron is $X = \{\dots, 1, 0, 1, 0, 1, \dots\}$, that is, $\langle X \rangle = 1/2$.

We can obtain the transition line $W_{SR}(h)$ [or $g_{SR}(Y)$] where the cycle-2 appear. Inserting the condition $\rho_{SR} = 1/2$ in equations (10) and (11) for ρ^+ , we get:

$$W_{SR} = \frac{2}{\Gamma} - 2h, \quad (38)$$

$$g_{SR} = \frac{p}{q} - \frac{2}{q\Gamma J} + \frac{2h}{qJ} = g_c - \frac{1}{q\Gamma J} + \frac{2(Y-1)}{qJ}. \quad (39)$$

The result for W_{SR} is coherent with previous results for cycle-2 obtained in [36]. If $\Gamma J \gg 1$, the SR phase occurs for $g < g_c \approx 4$, independently of Y , which is similar to Brunel's phase diagram [5]. For moderate ΓJ , the transition line is

$$Y_{SR}(g) = 1 + \frac{1}{\Gamma} - \frac{pJ}{2} (1 - g\gamma), \quad (40)$$

where $\gamma = q/p$ (see Fig. 3d).

3. Transition between irregular spiking states

Synchronous irregular (SI) appears as inhibition is increased from an asynchronous irregular (AI) phase through a flip bifurcation with small amplitude. For a map of the form $\rho[t + 1] = F(\rho[t])$, the bifurcation condition is given by:

$$\left. \frac{dF}{d\rho} \right|_{\rho^+} = -1. \quad (41)$$

where ρ^+ is the fixed point given by equation (10). Simplifying the terms in the last equation, we obtain:

$$Y_F = 1 - \frac{1}{\Gamma} - W + \frac{2}{\Gamma} \sqrt{1 + \Gamma W}, \quad (42)$$

$$= 1 - \frac{1}{\Gamma} + pJ(g\gamma - 1) + \frac{2}{\Gamma} \sqrt{1 - \Gamma pJ(g\gamma - 1)}. \quad (43)$$

These bifurcations lines are shown in Fig. 3d.

For large $g > g_c$, the iteration of the $\rho[t]$ map returns $0, \Gamma(Y - 1), 0, \Gamma(Y - 1), \dots$; this is a solution of equation (30). This solution is also cycle-2, but its $\rho[t] < 0$ part is cut off by the step function. To obtain it, we impose $\rho[t + 2] = \rho[t] = 0$. This implies that:

$$\rho[t + 2] = (1 - \rho[t + 1])\Gamma(h + W\rho[t + 1]), \quad (44)$$

$$= (1 - \Gamma h)\Gamma(h + W\Gamma h) = 0. \quad (45)$$

Solving this equation, we find that this cycle appears for $g > g_0$, with g_0 given by

$$\Gamma W_0 = -1, \quad (46)$$

$$g_0 = \frac{p}{q} + \frac{1}{q\Gamma J} = g_c + \frac{2}{q\Gamma J}. \quad (47)$$

4. Low activity state with respect to the external current

We can also examine the behavior for fixed $g > g_c$ as a function of input Y . We obtain an almost linear behavior similar to that found by Brunel [5], see Fig. 3b. A first order expansion for large J in equation (11) gives:

$$\rho(Y) \approx \frac{Y - 1}{Jp(g\gamma - 1) + (Y - 1) + 1/\Gamma} \Theta(Y - 1) \approx \frac{Y - 1}{Jp(g\gamma - 1)} \Theta(Y - 1). \quad (48)$$

Equation (48) has the correct maximum limit $\rho \rightarrow 1$ when $Y \rightarrow \infty$. For moderate values of Y , equation (48) presents the linear behavior found in equation (24) of Brunel [5].

Due to leakage, the curves of Brunel [5] start at $Y = 1 - \mu$ and have some curvature, in contrast to our linear $\rho \propto (Y - 1) \Theta(Y - 1)$ behavior (since we used $\mu = 0$ in Fig. 3b). But it is possible to obtain curves that start at $Y = 1 - \mu$ with curvature similar to Brunel [5], using the solution for $\mu > 0$ below.

D. Active state for nonzero leakage

The stationary firing rates for general μ are valid in two limits: either close to the critical region or close to the saturating regime, i.e. when the potential of the first peak in the distribution $P_t(V)$ approaches $V_S = 1/\Gamma + \theta$.

When $\mu > 0$, the active phases must be described by the recurrence equations for both excitatory and inhibitory populations. Using the simplified weight, we can rewrite the recurrence equations (19), (20) and (21) in the stationary state as:

$$\rho = \sum_{k=1}^{\infty} \eta_k \Phi(U_k), \quad (49)$$

$$\eta_k = \eta_{k-1} (1 - \Phi(U_{k-1})), \quad (50)$$

$$U_k = \mu U_{k-1} + W\rho + I = (W\rho + I) \sum_{n=0}^{k-1} \mu^n \quad (51)$$

$$= (W\rho + I) \frac{1 - \mu^k}{1 - \mu}, \quad (52)$$

with $U_0 = 0$ because we consider the resting potential to be equal to the reset potential. Substituting equations (51) and (50) in (49) and changing indexes yields:

$$\rho = \sum_{k=0}^{\infty} \eta_k (1 - \Phi(U_k)) \Phi(\mu U_k + W\rho + I).$$

Close to the critical point, where the stationary potentials belong to the linear part of the firing function, *i.e.* $\theta < U_1 < U_\infty < V_S$, where U_∞ is the limit potential of “infinite firing age” $U_\infty = \frac{W\rho + I}{1 - \mu}$. In this case:

$$\rho = \sum_{k=0}^{\infty} \eta_k (1 - \Phi(U_k)) \Gamma(\mu U_k + W\rho + I - \theta).$$

By using the relation in equation (49) and the normalization $\sum_{k=0}^{\infty} \eta_k = 1$ we obtain:

$$\rho = -\Gamma W \rho^2 + \rho(\mu + \Gamma W - \Gamma(I - \theta)) + \Gamma \tilde{h} - \Gamma \mu \sum_{k=0}^{\infty} \eta_k \Phi(U_k) U_k,$$

where $\tilde{h} = I - (1 - \mu)\theta$. Using equation (52) to describe U_k only outside of the Φ function argument in the sum of the last term, leads to:

$$\frac{\Gamma W}{1 - \mu} \rho^2 + \rho(1 - \mu + \frac{\Gamma \tilde{h}}{1 - \mu} - \Gamma W) - \Gamma \tilde{h} - \frac{\mu(W\rho + I)}{1 - \mu} \sum_{k=0}^{\infty} \eta_k \Phi(U_k) \mu^k = 0, \quad (53)$$

that holds when all stationary potentials lie in the linear region of the Φ function, i.e., when $U_1 > \theta$ and $U_\infty < V_S$. Note that in the case $\mu = 0$, the above equation becomes equation (5).

When the system is close to the critical value, we can consider the last term to be negligible for $\mu < 1$, because $\Phi(U_1)$ goes to zero as U_1 approaches θ . In this case, we can use:

$$\frac{\Gamma W}{1 - \mu} \rho^2 + \rho(1 - \mu + \frac{\Gamma \tilde{h}}{1 - \mu} - \Gamma W) - \Gamma \tilde{h} = 0. \quad (54)$$

When $\tilde{h} = 0$, there is a second order phase transition because the solutions to equation (54) are $\rho^- = \rho^* = 0$ and

$$\rho = \frac{W - W_c}{W} (1 - \mu), \quad (55)$$

where

$$W_c = \frac{(1 - \mu)}{\Gamma}. \quad (56)$$

This relation can also be rewritten as:

$$\rho = \frac{g_c - g}{p/q - g} (1 - \mu), \quad g_c = p/q - \frac{1 - \mu}{q\Gamma J}, \quad (57)$$

in good approximation close to the critical point ($g \lesssim g_c$).

As ρ approaches 1/2, when $U_1 \geq V_S$, the $\mu > 0$ case is equivalent to the $\mu = 0$ case. When $U_1 < V_S$ but $U_2 > V_S$, the stationary potentials distribution has three peaks. We can then solve equation (49) with the normalization $\eta_2 = 1 - \eta_0 - \eta_1 = 1 - 2\rho$. Using this constraint in equation (50) we obtain an equation that, interestingly, does not depend on μ :

$$\Gamma W \rho^2 + \rho(\Gamma h - 3) + 1 = 0, \quad (58)$$

that provides an exact solution for the firing rate for the case $\mu > 0$:

$$\rho^\pm = \frac{3 - \Gamma h \pm \sqrt{(3 - \Gamma h)^2 - 4\Gamma W}}{2\Gamma W}, \quad (59)$$

that converges to $\rho^* = 1/2$ as $U_1 \rightarrow V_S$.